Chemical origin of nanoscale polar domains in PbZn$_{1/3}$Nb$_{2/3}$O$_3$

T. R. Welberry[*] and D. J. Goossens

Research School of Chemistry, Australian National University, Canberra, ACT 0200, Australia

M. J. Gutmann

ISIS Facility, Rutherford Appleton Laboratory, Chilton, Didcot, Oxon, United Kingdom

We describe the development of an atom-based Monte Carlo simulation model which gives rise to a nanoscale polar domain structure as envisaged to occur in Pb(Zn$_{1/3}$Nb$_{2/3}$)O$_3$ (PZN) and similar relaxor ferroelectric materials. Individual domains are essentially thin platelike domains normal to each of the six $\langle 110 \rangle$ directions. Calculated diffuse scattering patterns have been obtained from the simulations, and these are in good agreement with observed neutron scattering data. Nanoscale domain formation is driven by the need for the Pb atoms to satisfy their valence requirements; within a planar domain, the Pb atoms are displaced in a concerted fashion away from the center of their 12-fold coordination polyhedra with an in-plane displacement along $\langle 110 \rangle$ towards one of the coordinating O atoms. The *B*-site cations Zn and Nb display a strong tendency to alternate in the $\langle 100 \rangle$ directions but complete order is frustrated by the 2:1 stoichiometry. No diffraction evidence has been found that this *B*-site ordering is directly linked to the nanoscale polar domain ordering. Such a linkage cannot be completely ruled out, but if it does exist, its effect on the diffraction pattern must be quite subtle. The *B*-site ordering does play an indirect role in establishing the average cell dimension, which in turn dictates the magnitude of the Pb displacements. The effect of applying an external electric field is modeled, and the results are found to be consistent with experiment.

PACS number(s): 77.84.−s, 61.12.−q

I. INTRODUCTION

Relaxor ferroelectrics have attracted tremendous attention in recent years because of their extraordinary dielectric and piezoelectric properties.[1] Of these materials the lead-based perovskite relaxor Pb(Zn$_{1/3}$Nb$_{2/3}$)O$_3$ (PZN) [together with its sister compound Pb(Mn$_{1/3}$Nb$_{2/3}$)O$_3$ (PMN)] has been one of the most extensively studied relaxor systems.[2,3] These materials are a crucial component in transducers that convert between mechanical and electrical energies, such as in ultrasonic devices.[4] Despite this extensive study the exact nature of their structure and how it relates to their properties is still poorly understood.

Relaxor systems generally are marked by a broad maximum and a strong frequency dependence of their dielectric permittivity. It is generally accepted that their structure at temperatures well above the Curie temperature is comprised of nanometer-sized polar domains or nanoregions[5] (PNR's), and it is widely believed that these play an essential role in the relaxor properties.[6] Although the existence of PNR's in relaxors is well documented, their structure and origin are still the subject of controversy. For example, while it is accepted that a key feature of the nanoscale domain structure is that the Pb^{2+} ions are displaced from the average site position at the center of the coordination shell of oxygen atoms, there is little consensus as to whether the displacements are in the $\langle 111 \rangle$, $\langle 110 \rangle$, or $\langle 100 \rangle$ direction. Woodward and Baba-Kishi[7] claim that it should be $\langle 111 \rangle$, and Dmowski *et al.*[8] using pair-density function analysis found the $\langle 100 \rangle$ direction to be the most likely, while in an earlier paper we presented evidence from neutron diffuse scattering experiments that the displacements must be in the $\langle 110 \rangle$ direction.[9]

Diffuse scattering is one of the few techniques that is able to probe local structural detail like that found in PZN. Although x-ray diffuse scattering has advantages in terms of available flux and hence the ability to make use of small samples, neutron diffuse scattering is of benefit for oxide materials containing heavy metals since the neutron cross section for oxygen is comparable to those for the metal ions. In a previous paper[9] we reported experiments in which neutron diffuse scattering data were recorded for PZN at ambient temperature using a neutron time-of-flight Laue diffractometer. Three sections of the data from this study are reproduced in Fig. 1 for reference.

Monte Carlo (MC) computer simulation of a model structure has become a powerful and well-accepted technique for aiding the interpretation and analysis of diffuse scattering patterns.[10,11] The method consists of comparing diffraction patterns calculated from a computer model of the disordered structure with measured x-ray or neutron diffuse intensities. The advantage of the method is that it can be applied generally to all systems regardless of their complexity or the size of the atomic displacements that might be present. The only limitation is the extent to which the MC energy can be made to realistically represent the real system energy. At one extreme a very simplified model may be useful in demonstrating particular qualitative effects[12] while at the other a quantitative and very detailed description of a disordered structure can be obtained.[13]

In previous work[9] a fairly simplistic and rather artificial approach was taken in order to demonstrate a number of key effects that give rise to distinctive features in the diffuse scattering data of PZN. The study did not attempt to establish a realistic set of interatomic potentials that could account for the scattering but simply used sets of interacting random variables to represent the various atomic shifts. The MC simulation was used to introduce correlations between these
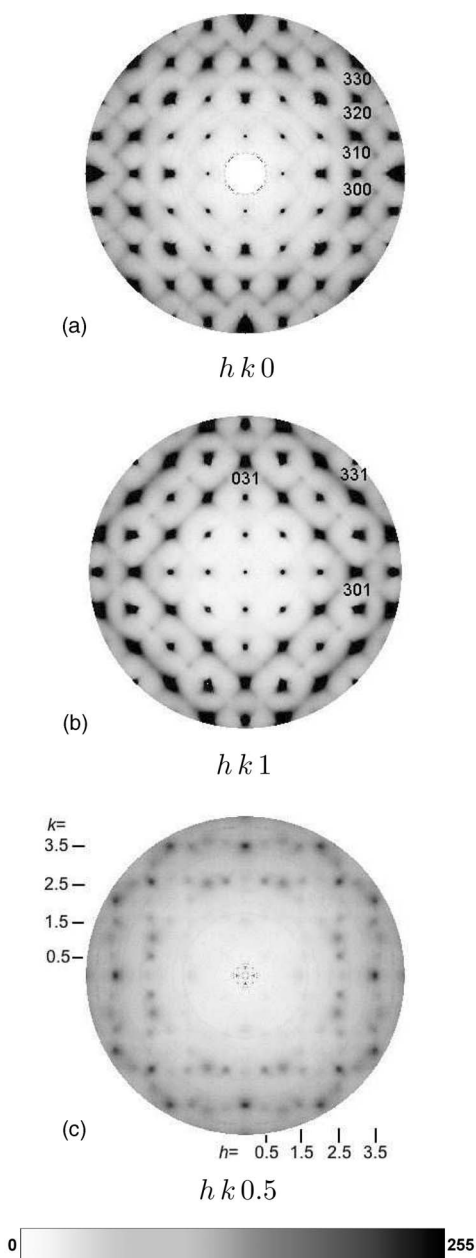
(a)

$h\,k\,0$

(b)

$h\,k\,1$

(c)

$h\,k\,0.5$

FIG. 1. Three sections of neutron diffuse scattering taken from a complete 3D volume recorded on the SXD time-of-flight instrument at ISIS [see Welberry *et al.* (Ref. 9)]. Darker gray scale indicates higher scattered intensity.
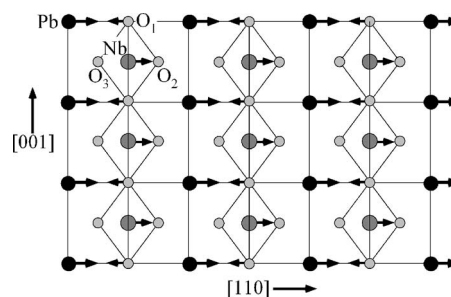

FIG. 2. The envisaged displacement patterns for the different ions in the nanoscale polar domains in PZN [see Welberry *et al.* (Ref. 9)].

the azimuthal variation of the intensity in the diffuse rods. In Fig. 1(a) it is seen that the diffuse rod corresponding to $h+k=0$ has zero intensity. This is a systematic extinction that necessarily implies that the atomic displacements giving rise to the $h+k=n$ rods must be directed along $[1\bar{1}l]$. The fact that the same extinction condition is also present in Fig. 1(b), however, shows that l must equal zero. I.e., the atomic displacements giving rise to the $h+k=n$ rods must be directed along $[1\bar{1}0]$. Similarly, the zero intensity of the $h-k=0$ diffuse rod in Figs. 1(a) and 1(b) necessarily implies that the atomic displacements that give rise to the $h-k=n$ rods are directed along $[110]$.

In order to account for the relative intensities of different orders of the diffuse rods it is necessary that the B cations (Nb/Zn) tend to be displaced in phase with the Pb^{2+} ions, while the O^{2-} ion occurring between any two Pb^{2+} ions is displaced out of phase. This essentially means that along the $\langle 110 \rangle$ direction within the nanoscale domain the Pb^{2+} ion makes one long bond and one short bond. Figure 2 shows schematically the envisaged ionic displacement patterns within a domain.

A second key fact that was established by the study was that the B cations are locally ordered with a tendency for Nb and Zn to alternate along each of the three cubic axial directions, although because of the 2:1 stoichiometry this alternation cannot be perfect. The range of this short-range order is comparable to the range of order in the nanoscale polar domains, as witnessed by the full widths at half maximum (FWHM) of the two types of diffuse peak in the $hk0.5$ data shown in Fig. 1(c) (those for which $h\pm k=n$ are due to occupancy ordering and those for which $h\pm k=n+\frac{1}{2}$ are due to the intersection of the diffuse rods), but there did not appear to be any evidence that the two were directly linked.

More recently Xu *et al.*[14] have reported experiments in which diffuse x-ray scattering was observed as a function of applied electric field. Although these authors appear to be in agreement with Welberry *et al.*,[9] regarding the thinness and the orientation of the planar domains, they described the domains as having a "pancake" shape. In addition they expressed surprise that this local domain structure and the diffuse scattering in the form of the rods parallel to $\langle 110 \rangle$ persisted when long-range $[111]$-polarized ferroelectric order was induced by an electric field applied along $[111]$.

In this paper we report on an extension of the previous work.[9] In that work we used sets of interacting random

shifts in order to demonstrate the origin of the different diffraction features that were observed.

Using this approach it was possible to generate various attributes of the nanoscale domain structure and assess the effect of these on the calculated diffraction patterns by comparison with the observed neutron data.

Although this work was only qualitative in nature, it clearly established that the basic nanoscale domains in PZN were thin sheetlike domains oriented normal to each of the six $\langle 110 \rangle$ directions. Within each domain the Pb^{2+} ion displacements are all directed in a concerted way along another $\langle 110 \rangle$ direction and normal to $\langle 001 \rangle$ (within the plane of the domain). This displacement direction is required to explain

variables to represent atomic displacements in a rather artificial manner. In the present work we attempt to develop a more realistic atom-based MC model of the nanoscale domain structure. This approach is expected to yield calculated diffraction patterns that are in better agreement with the observed data and also provide insight into how the six differently oriented types of nanoscale domain can pack together in three dimensions. In addition such a model provides a means of exploring and understanding what happens when an external electric field is applied to the system.

II. CHEMICAL ORIGIN OF THE NANOSCALE DOMAIN STRUCTURE

The so-called "bond-valence sum" or "apparent valence" method[15] is widely used in solid-state chemistry to assess whether the individual valencies of the constituent atoms (or ions) in a solid are satisfied on a local level. There exist empirical parameters R_{ij} and b that are transferable between many classes of compounds and that enable the apparent valence V_i of a given ion i to be calculated from the bond distances d_{ij} to its j neighbors:

$$V_i = \sum_j \nu_{ij}, \tag{1}$$

where

$$\nu_{ij} = \exp[(R_{ij} - d_{ij})/b]. \tag{2}$$

A. Pb ion displacements

If such a sum as Eq. (1) is calculated for the Pb ion at the center of its coordination polyhedron of 12 oxygens in the average unit of PZN, it is found that the apparent valence is only 1.503 compared to the actual valence of Pb of 2. This means that the Pb atom is strongly underbonded and must move away from the average position in order to increase this sum. Such a displacement is shown in Fig. 3(a). Table I shows the separate contributions to the Pb apparent valence from the 12 surrounding O^{2-} ions for two cases: when the Pb ion is at the center of the coordination polyhedron and when it is moved along a ⟨110⟩ direction towards one of the O^{2-} ions (No. 12) and away from the opposite ion (No. 1) [see Fig. 3(a)]. The values given correspond to a Pb shift of $0.141a_0 = 0.576$ Å, where $a_0 = 4.073$ Å is the cubic cell edge. It should be noted that this estimate of the Pb ion displacement required is made with the assumption that all the O^{2-} ions remain on their average sites. Since the previous study[9] indicated that the O(12) would move towards the Pb, the actual magnitude for the Pb shift would be expected to be somewhat less than this.

B. Concerted Pb shifts along ⟨110⟩

It is not just the Pb apparent valence that has to be satisfied. All of the ions in the structure will shift in order to try to satisfy their own apparent valence as closely as possible. Satisfying such an intricately connected and complex set of constraints for all the ions in the disordered structure is a
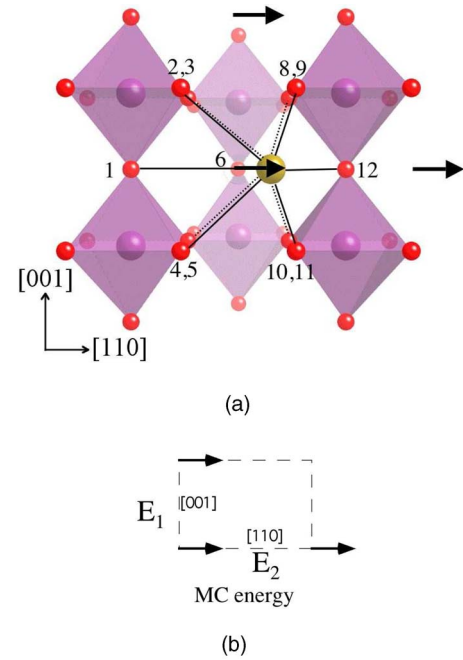

(a)

(b)

FIG. 3. (Color online) (a) View down $[1\bar{1}0]$ of the 12-fold coordination of the Pb ion. Black arrows indicate the proposed off-center displacements. (b) The Monte Carlo energies E_1 (connecting neighbors in the [001] direction) and E_2 (connecting neighbors in the [110] direction), which promote the formation of domains in which neighboring displacements in the [110] and [001] directions tend to be parallel.

complex problem in cooperation that is beyond the scope of the present study. However, one aspect of the cooperation is easy to demonstrate. As the Pb atom moves towards O(12) the apparent valence for O(12) is increased and the atom becomes overbonded. This means that it will in turn be reluctant to share its electrons with the next-neighboring Pb atom. This causes the distance to this next Pb to increase, which can only be achieved if the displacement of this second Pb ion is in the same direction as the first.

C. B-cation ordering

The bond-valence method can also be used to assess how well the valencies of the Nb^{5+} and Zn^{2+} ions are satisfied within the observed average structure. It is found that when placed at the center of the average regular octahedron of O^{2-} ions Nb is greatly underbonded while Zn is overbonded. As a

TABLE I. Contributions ν_{ij} to the bond-valence sum V_i for Pb from its 12 oxygen neighbors for the two cases: Pb at the center of polyhedron and Pb displaced by 0.576 Å along [110]. The individual contributions ν_{ij} are calculated using Eq. (2) with values of R_{ij} and b taken from Brese and O'Keeffe (Ref. 15).

Neighbor	1	2,3,4,5	6,7	8,9,10,11	12	V_i
ν_{ij}, no shift	0.125	0.125	0.125	0.125	0.125	1.503
ν_{ij}, [110] shift	0.026	0.052	0.107	0.240	0.594	2.002

TABLE II. Definition of the n basic displacements along x, y, and z for the 12-state vector quantity Ψ_n representing the Pb ions.

n	1	2	3	4	5	6	7	8	9	10	11	12
x	0	0	0	0	δ	δ	$-\delta$	$-\delta$	δ	δ	$-\delta$	$-\delta$
y	δ	δ	$-\delta$	$-\delta$	0	0	0	0	δ	$-\delta$	δ	$-\delta$
z	δ	$-\delta$	δ	$-\delta$	δ	$-\delta$	δ	$-\delta$	0	0	0	0

measure of this, for the apparent valence of Nb to be 5.0 the cell dimension a_0 must be reduced from the observed value of 4.073 Å to a value of 3.955 Å, a reduction of 2.9%. Conversely for the apparent valence of Zn to be 2.0 the cell dimension must increase to 4.218 Å, an expansion of 3.5%. This provides a strong driving force for the Nb^{5+} and Zn^{2+} ions to undergo local ordering in which Nb and Zn tend to alternate. By alternating, any strain that is induced by the expansion around Zn is almost completely compensated within a one-unit-cell repeat of the contraction around Nb. Because of the 2:1 stoichiometry of Nb to Zn, this alternation cannot be perfect but substantial short-range order (SRO) can be achieved (see Sec. III C), which will minimize any strain.

III. MONTE CARLO MODEL

A. Pb ordering

It is clear from the discussions in Sec. II that the $\langle 110 \rangle$-type Pb ion displacement away from its average site at the center of the 12-fold coordination polyhedron is the driving force for the nanoscale domain structure. In order to develop a suitable MC potential to produce locally ordered domains we therefore represent each Pb ion as a 12-state vector quantity $\Psi_n(i,j,k)$, where i,j,k are indices defining a primitive cubic lattice (see Table II). The arguments in Sec. II B explain why these displacements should be correlated along $\langle 110 \rangle$ rows. However, it is clear from the diffraction evidence that the Pb displacements must also be correlated laterally (along [001]), as shown in Fig. 2, to form planar domains. We therefore attempt to build a simple potential which will tend to induce correlations within planes normal to $[1\bar{1}0]$ both along [110] and along [001].

The energy of the pth Pb ion due to interaction in the plane perpendicular to $[1\bar{1}0]$ is given by

$$E^p_{[1\bar{1}0]} = \sum_{\substack{[001] \text{ in-plane} \\ \text{neighbors, } q}} E^{pq}_1 + \sum_{\substack{[110] \text{ in-plane} \\ \text{neighbors, } r}} E^{pr}_2, \tag{3}$$

where

$$E^{pq}_1 = \begin{cases} E_1 & \text{if } \Psi^p \parallel \Psi^q \parallel \pm[110], \\ 0 & \text{otherwise}, \end{cases}$$

$$E^{pr}_2 = \begin{cases} E_2 & \text{if } \Psi^p \parallel \Psi^r \parallel \pm[110], \\ 0 & \text{otherwise}. \end{cases} \tag{4}$$

E^{pq}_1 and E^{pr}_2 are energies defining the interaction between the vectors representing the Pb displacements on neighboring

sites as shown in Fig. 3(b). E^{pq}_1 is zero unless both the target Pb atom (p) and its [001] neighbor (q) are displaced along [110] (or both are displaced along $[\bar{1}\bar{1}0]$), when it takes on value E_1, which is some constant. Similarly E^{pr}_2 is zero unless both the target Pb atom (p) and its [110] neighbor (r) are displaced along [110] (or both are displaced along $[\bar{1}\bar{1}0]$).

A similar potential can be used to induce order in other symmetry-related planes. To induce local order in planes normal to $[01\bar{1}]$ a similar MC energy of the form

$$E^p_{[01\bar{1}]} = \sum_{\substack{[100] \text{ in-plane} \\ \text{neighbors, } q}} E^{pq}_1 + \sum_{\substack{[011] \text{ in-plane} \\ \text{neighbors, } r}} E^{pr}_2 \tag{5}$$

can be used. Here E^{pq}_1 is zero unless both the target Pb atom and its [100] neighbor are displaced along $\pm[011]$ and E^{pr}_2 is zero unless both the target Pb atom and its [011] neighbor are displaced along $\pm[011]$.

In addition to Eqs. (3) and (5) there are four more similar equations appropriate to ordering in planes normal to [110], [011], [101], and $[10\bar{1}]$.

In order to induce local order in all six orientations simultaneously a total energy for atom p of the form

$$E^p_{\text{total}} = E^p_{[011]} + E^p_{[01\bar{1}]} + E^p_{[101]} + E^p_{[10\bar{1}]} + E^p_{[110]} + E^p_{[1\bar{1}0]} \tag{6}$$

can be used. This form of the MC energy was used for the ordering of Pb displacements in the simulations that are described later in this paper. This form is seen to contain only terms that lie within each $\langle 110 \rangle$ plane of the nanoscale domains, and it is implicit in this that the ordering in one such nanoscale domain is independent of the $\langle 110 \rangle$ plane immediately above or below. In order to investigate the effect of allowing out-of-plane interactions some examples were generated using a modified form of Eq. (3) (and its symmetry equivalents):

$$E^p_{[1\bar{1}0]} = \sum_{\substack{[001] \text{ in-plane} \\ \text{neighbors, } q}} E^{pq}_1 + \sum_{\substack{[110] \text{ in-plane} \\ \text{neighbors, } r}} E^{pr}_2 + \sum_{\substack{[100],[010] \\ \text{neighbors, } s}} E^{ps}_3$$

$$+ \sum_{\substack{[200],[020] \\ \text{neighbors, } t}} E^{pt}_4. \tag{7}$$

B. "Size-effect" relaxation

In Sec. III A the $\Psi_n(i,j,k)$ variables were considered to reside precisely on the sites of a simple cubic lattice and so the atomic shifts defined in Table II represent the only departures from the average site positions. In later sections we show diffraction patterns calculated from MC simulations in which this is strictly the case. However, in all real disordered solids any occupancy distribution is always accompanied by local "size-effect" relaxations.[9] In this case, although each Pb displacement is nominally obtained by selecting one of the shifts from Table II, it is expected that on any given site the shifts will be modified depending on the values of $\Psi_n(i,j,k)$ for the neighboring sites:

$$E_{\text{size}} = \sum_{\substack{\langle 100 \rangle \\ \text{vectors}}} [d_{m,n} - a_0(1 + \zeta_{m,n})]^2 + \sum_{\substack{\langle 110 \rangle \\ \text{vectors}}} [d_{m,n} - \sqrt{2}a_0$$

$$\times (1 + \epsilon_{m,n})]^2. \tag{8}$$

Here $\zeta_{m,n}$ and $\epsilon_{m,n}$ are size-effect parameters which are applied along $\langle 100 \rangle$ and $\langle 110 \rangle$ vectors, respectively. The indices m and n refer to the respective Ψ_n and Ψ_m connected by the vector. $d_{n,m}$ is the current length of the vector in the simulation. In the present study it has been assumed for simplicity that both $\zeta_{m,n}$ and $\epsilon_{m,n}$ are related to the scalar product, $P = \Psi_m \cdot \Psi_n$, of the two displacement vectors: e.g.,

$$\epsilon_{m,n} = k_{\langle 110 \rangle} P/(2\delta^2),$$

$$\zeta_{m,n} = k_{\langle 100 \rangle} P/(2\delta^2). \tag{9}$$

Here $k_{\langle 110 \rangle}$ is a constant defining the magnitude of the effect for $\langle 110 \rangle$ vectors and $k_{\langle 100 \rangle}$ for $\langle 100 \rangle$ vectors.

C. *B*-cation ordering

In Sec. II C arguments were presented for expecting local ordering on the perovskite *B* sites with Nb and Zn tending to alternate. Such local ordering was achieved in the simulations presented here by using a simple Ising model with a MC energy of the form

$$E_{B \text{ site}} = \sum_{\substack{\text{all} \langle 100 \rangle \\ \text{vectors}}} J\sigma_m \sigma_n. \tag{10}$$

Here σ_m and σ_n are $(+1/-1)$ Ising spin variables at sites m and n, respectively, on the primitive cubic *B*-site lattice. Antiferromagnetic ordering close to maximal for 2:1 stoichiometry was achieved by assigning a large positive value for J/kT of 10 000.

In the resulting distribution the alternation of Zn and Nb only exists over a short range. Zn will almost always be succeeded by Nb, whereas Nb may be followed by Nb or Zn. This is similar to the random-site model put forward by Akbas and Davies[16] in that it satisfies the stoichometric composition on a local scale and does not result in nanolevel phase separation and compositional segregation. It is different in that it does not suggest there are two kinds of *B* sites, one occupied by Nb and the other by a mixture of Nb and Zn, and in that it does not imply randomness on the *B* sites so much as finite-ranged correlations, which to a Bragg diffraction experiment will *appear* random.

Since this aspect of the disorder in PZN was not the main focus of the present work, the same occupancy distribution of Nb and Zn achieved by this means was used in all the simulations described below.

D. Inclusion of other ions

Although the main driving force for the local ordering in PZN are the Pb displacements described in Sec. II A, it is necessary to include the other ions in the model since their presence substantially affects the observed diffraction patterns. For the purposes of the present study the inclusion of these other ions has been carried out by tying them in a deterministic way to the positions of the Pb ions which were generated by the MC simulation using Eqs. (6) and (8). If $X_{i,j,k}$, $Y_{i,j,k}$, and $Z_{i,j,k}$ are the resulting displacements of the Pb atom away from the average site position (at $0,0,0$) along the three axial directions x, y, and z in the (i,j,k)th cell, then the coordinates for the Nb or Zn ion in the (i,j,k)th cell were set to

$$X_{i,j,k}^{\text{Nb/Zn}} = [X_{i,j,k} + X_{i+1,j,k} + X_{i,j+1,k} + X_{i,j,k+1} + X_{i+1,j+1,k}$$
$$+ X_{i,j+1,k+1} + X_{i+1,j,k+1} + X_{i+1,j+1,k+1}]/8.0 + 0.5,$$

$$Y_{i,j,k}^{\text{Nb/Zn}} = [Y_{i,j,k} + Y_{i+1,j,k} + Y_{i,j+1,k} + Y_{i,j,k+1} + Y_{i+1,j+1,k}$$
$$+ Y_{i,j+1,k+1} + Y_{i+1,j,k+1} + Y_{i+1,j+1,k+1}]/8.0 + 0.5$$

$$Z_{i,j,k}^{\text{Nb/Zn}} = [Z_{i,j,k} + Z_{i+1,j,k} + Z_{i,j+1,k} + Z_{i,j,k+1} + Z_{i+1,j+1,k}$$
$$+ Z_{i,j+1,k+1} + Z_{i+1,j,k+1} + Z_{i+1,j+1,k+1}]/8.0 + 0.5. \tag{11}$$

For placing the O ions in a deterministic way a method was used similar to that described previously.[9] The aim here was to ensure that the displacement of a particular O^{2-} ion was in the opposite direction to that of the neighboring Pb ion. For the O_1 ion, nominally at $(0.5,0.5,0)$, the coordinates were obtained as

$$X_{i,j,k}^{O_1} = -[X_{i,j,k} + X_{i+1,j,k} + X_{i,j+1,k} + X_{i+1,j+1,k}]/4 + 0.5,$$

$$Y_{i,j,k}^{O_1} = -[Y_{i,j,k} + Y_{i+1,j,k} + Y_{i,j+1,k} + Y_{i+1,j+1,k}]/4 + 0.5,$$

$$Z_{i,j,k}^{O_1} = +[Z_{i,j,k} + Z_{i+1,j,k} + Z_{i,j+1,k} + Z_{i+1,j+1,k}]/4. \tag{12}$$

Similar expressions for the O_2 and O_3 ions, nominally at $(0,0.5,0.5)$ and $(0.5,0,0.5)$, can be written down by inspection. It should be noted that the $Z_{i,j,k}^{O_1}$ term in Eq. (12) corresponds to displacements tangential to the Pb-Pb vectors on which the oxygen resides. The + sign means that the motion of the oxygen in this tangential direction follows that of the supporting Pb ions. However, since this tangential motion is small compared to that along the Pb-Pb vectors, this term has little effect on the diffraction patterns.

IV. MC SIMULATIONS

Monte Carlo simulations were carried out using a model crystal comprising $48 \times 48 \times 48$ unit cells. As described above the basic MC modeling was carried out using the Pb atom arrays and all other atom positions were obtained in a deterministic way from these. The simulations were carried out in four stages: stage 1, which was only carried out once used Eq. (10) to establish a distribution of Nb/Zn occupancies. In stage 2 the basic ordering of the differently oriented Pb displacements was carried out using Eq. (6). In stage 3 the Pb positions from stage 2 were allowed to relax using the "size-effect" parameters [Eqs. (8) and (9)]. Finally in stage 4 the remaining atom coordinates were derived using Eqs. (11)

and (12). From these final coordinates calculated diffraction patterns were computed using the program DIFFUSE.[17] It should be noted that DIFFUSE calculates only the diffuse scattering component of the scattered intensity distribution. The Bragg component is removed by subtracting the contribution of the average lattice.

In carrying out the stage 2 simulations the array of Pb displacement variables, $\Psi_n(i,j,k)$, was first set up randomly so that any one site had an equal probability of containing Pb displaced in one of the 12 different directions. In order to maintain the overall fractions of each type of displacement at each MC step the variables on two randomly chosen sites were interchanged, with the system energy being computed before and after. For all of the stage 2 simulations 200 cycles of MC simulation were carried out, where a cycle is that number of individual steps required to visit each site once on average.

The normal Metropolis algorithm[18] was used throughout. Although during the preliminary stages of the study numerous different conditions were tried, for the examples reported here the energies E_1 and E_2 of Eq. (4) were set to values of $E_1/k_BT=E_2/k_BT=-200$.

Figure 4 shows the result of this stage 2 ordering. (a) and (b) are two layers separated by $\sqrt{2}a_0$ along $[1\bar{1}0]$. It is evident that small nanoscale domains have formed which consist of either black (blue) arrows or of gray (pink) arrows. Comparison of (a) and (b) shows that the domains in one layer are essentially independent of those in the layer only one unit cell beneath or above. This confirms that the simple MC energy defined in Eqs. (3)–(6) has succeeded in producing distributions with the desired type of nanoscale domain structure. It should be stressed here that the distribution is statistically fully cubic and sections that appear similar to those shown in Fig. 4 may equally well be obtained in sections normal to any of the six $\langle 110 \rangle$ directions.

A. Calculated MC stage 2 diffraction patterns

In Fig. 5 we show calculated diffraction patterns corresponding to the distribution shown in Fig. 4 for both the $hk0$ and $hk1$ sections. These patterns show how the intensity occurring in the different diffuse rods (of the general form $h\pm k=n$) is dependent on the interference between the contributions from the different ions. Figures 5(a) and 5(b) show the $hk0$ and $hk1$ sections, respectively, calculated from the Pb ions alone. In this case both sections show rods $h\pm k=n$, for all $n\neq 0$. The absence of the $n=0$ rod is indicative of the $\langle 110 \rangle$ direction of the displacements. Figures 5(c) and 5(d) show the same sections when the Nb/Zn ions are also included in the calculation using Eq. (12). Here, in (c) the $h\pm k=2n$ rods are strong and the $h\pm k=2n+1$ rods are weak, while in (d) the $h\pm k=2n$ rods are weak while the $h\pm k=2n+1$ rods are strong. Figures 5(e) and 5(f) show the same sections with all ions present. Now, in (e), the $h\pm k=n$ rods are present for all $n\neq 0$, while for (f) we still have the $h\pm k=2n$ rods weak and the $h\pm k=2n+1$ rods strong. It should be stressed that all of these patterns are calculated with the coordinates obtained from the stage 2 MC calculations with each Pb displacement having one of
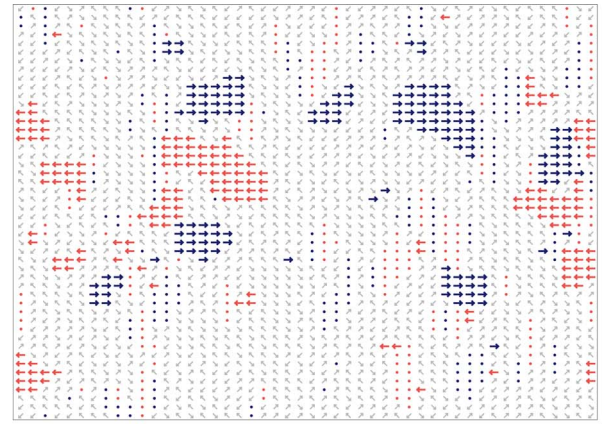
(a)
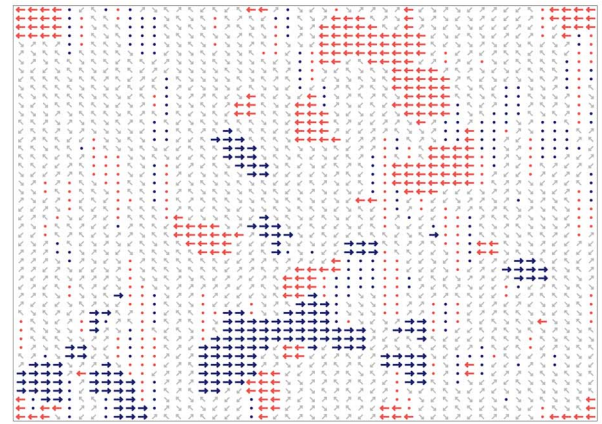
(b)

FIG. 4. (Color online) Distribution of Pb displacement vectors within one layer normal to $[1\bar{1}0]$ of the simulated structure. $[001]$ is vertical and $[110]$ is horizontal. The black (blue) and dark gray (pink) arrows are in-plane vectors directed along $[110]$ and $[\bar{1}\bar{1}0]$, respectively. Light gray arrows are out-of-plane $\langle 110 \rangle$ vectors, while small circles are vectors normal to the plane. (a) and (b) are two layers separated by $\sqrt{2}a_0$ along $[1\bar{1}0]$. Note that the correlated domains of black (blue) or dark gray (pink) arrows do not persist in successive layers, indicating that they are essentially thin platelike nanoscale domains.

the values given in Table II and the other ions having been inserted in a deterministic way using Eqs. (11) and (12).

Although the distributions in individual layers normal to $\langle 110 \rangle$ shown in Fig. 4 clearly show correlated nanoscale regions that do not persist in neighboring layers, it is instructive to view these distributions looking down $\langle 001 \rangle$, since that is the direction down which the computed sections have been calculated. Figure 6(a) shows one such layer for the same distribution as that in Fig. 4 together with the corresponding $hk0$ diffraction pattern. In this figure the nanoscale domains are seen edge on and appear as correlated rows of arrows extending in the $[110]$ and $[1\bar{1}0]$ directions. It is seen that these are not just single lines of arrows which would be

(a)

(b)

(c)

(d)

(e)

(f)

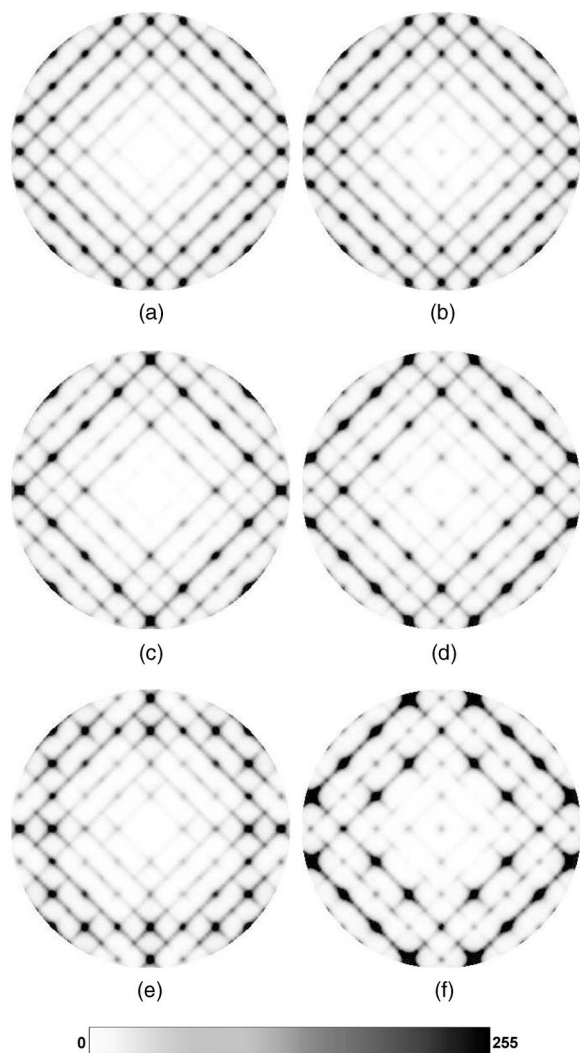0   255

FIG. 5. The effect of the different ions on the calculated diffraction patterns. (a), (b) were computed using Pb only; (c), (d) were computed using Pb and Nb/Zn; (e), (f) were computed using Pb, Nb/Zn, and O. (a), (c), and (e) are of the $hk0$ section; (b), (d), and (f) are of the $hk1$ section.
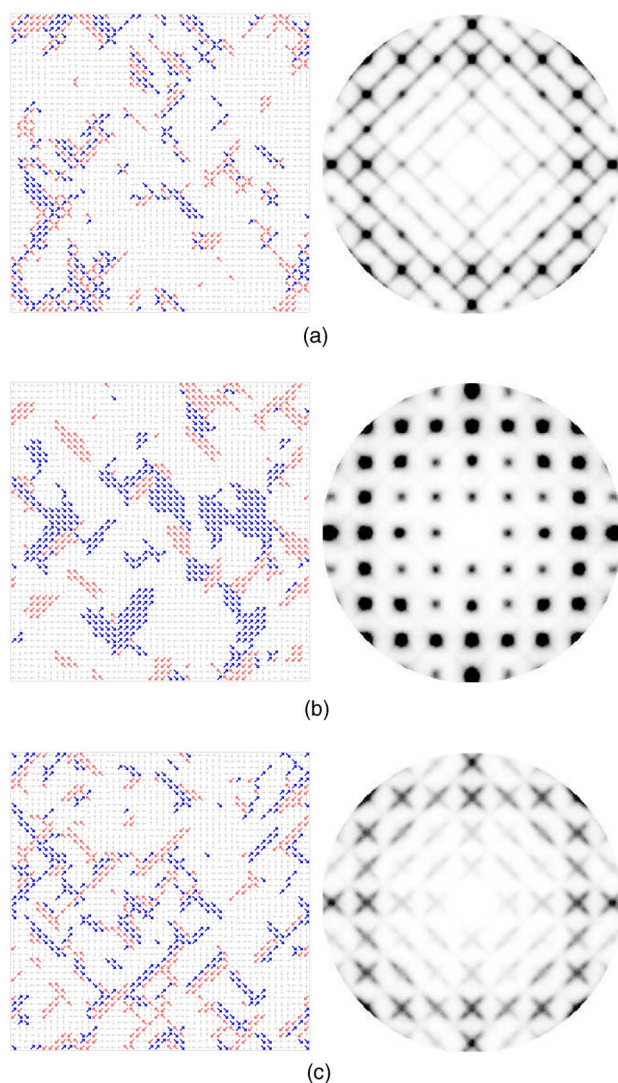

(a)

(b)

(c)

FIG. 6. (Color online) The effect of nanoscale domain thickness on the intensity distribution within the diffuse rods. The $hk0$ section diffraction patterns and a single layer of the real-space distribution viewed down [001], for models including (a) only in-plane interactions, (b) nearest-neighbor out-of-plane correlation, and (c) a tendency for double layers. [100] is vertical and [010] is horizontal.

the case if the nanoscale domains were strictly single layer. Rather the figure shows that there is a natural random variation of the thickness, even though there is no actual interaction promoting domains thicker than a single layer. This distribution corresponded to the values of the energies $E_1/k_BT = E_2/k_BT = -200$ and $E_3/k_BT = E_4/k_BT = 0$ [see Eq. (7)].

By adjusting the out-of-plane interactions E_3 and E_4 it is possible to control the average thickness of the domains. Two examples of this are shown in Figs. 6(b) and 6(c). For Fig. 6(b) the energy E_3 has been given a small negative value, thereby promoting the probability that the correlated Pb displacements within the layer will persist in the layers above and below. This tends to make three-dimensional domains and consequently in the diffraction pattern there is very little left of the rodlike diffuse scattering. For Fig. 6(c) the energy E_3 is again negative, promoting the continuation of the nanoscale domain in the third dimension, but this is then suppressed by having a positive value for E_4 which

prevents the order going beyond two layers. In this case the double-layer nanoscale domains are quite evident and this has had a marked effect on the distribution of intensity along the rods of intensity. These examples serve to illustrate that the model in which there are no out-of-plane interactions agrees most closely with the observations.

B. Size-effect relaxation

The diffraction patterns shown in Figs. 5 and 6 were all calculated after stage 2 MC simulation only. It can be seen in all cases that the diffraction features around all of the Bragg positions are symmetric, in marked contrast to the observed patterns of Fig. 1 where strong asymmetry can be seen—for example, around the 400 peak position. In order to try to reproduce these asymmetric effects we used Eqs. (8) and (9)

to carry out a stage 3 MC size-effect simulation. The distribution of Pb displacement vectors shown in Figs. 4 and 6(a) was used as a starting point for the relaxation. Although a variety of different values for $k_{\langle 100 \rangle}$ and $k_{\langle 110 \rangle}$ were tried, the best results were obtained when $k_{\langle 100 \rangle}=0$ and $k_{\langle 110 \rangle}=-0.04$. This corresponds to a distortion in which the MC algorithm tries to increase the length of the $\langle 110 \rangle$ vector connecting two Pb ions by 8% if the two Pb displacements are opposed to each other and similarly decreases the vector length if they are aligned.

Figure 7 shows three sections of the calculated diffraction pattern for this model. All three patterns show excellent qualitative agreement with the observed patterns of Fig. 1 and very much better agreement than those of the previous study.[9] In assessing the level of agreement it should be borne in mind that the model from which the patterns were calculated uses very few adjustable parameters. The first of these is the magnitude δ of the basic Pb shifts. For the example shown the value of δ was $0.05a_0$. It was found that a value of this magnitude was required in order that the row of diffuse peaks around the 300, 310, 320, and 330 Bragg positions all appeared more or less equally strong. For small values of δ the intensity of these peaks alternates between weak and strong. The second parameter chosen was the relative magnitude of E_1 and E_2. In this case they were chosen to be equal in order that the range of order within a given {110} plane was isotropic. Since the MC simulation was carried out at low temperature, the actual magnitudes of E_1 and E_2 were not critical, except in examples where E_3 and E_4 were also used. Finally the magnitude for the size-effect distortion parameter k_{110} was chosen in order to give an asymmetry of the diffuse peaks comparable to that observed. Significantly smaller values for k_{110} produced insufficient asymmetry, while significantly higher values resulted in the appearance of $h \pm k = 0$ diffuse rods of scattering which are systematically absent in the observations. This seemed to indicate that for high levels of distortion the ionic displacements were no longer along $\langle 110 \rangle$ which is required for the absence to be satisfied.

V. DISORDER IN AN APPLIED FIELD

There is considerable interest in exploring the effect of applying an external electric field to the current model, since PZN is a functional material.[14] We can study the effect of an applied field by applying a bias to the initial distribution of Pb shift vectors. For example, if we consider a field is applied along [111], we suppose that all Pb shifts that have a positive scalar product with [111] will occur more frequently and those with a negative scalar product will be less frequent. With this different initial distribution of Pb shift vectors the rest of the simulation is then carried out in an identical fashion. The actual frequencies used are given in Table III. It is seen that over two thirds of the crystal now has Pb ions displaced in one of only three directions [110], [101], and [011], each of which gives a positive scalar product with the [111] applied field direction.

The distributions resulting from this simulation are shown in Fig. 8. This figure should be compared to Fig. 4 corre-

(a)

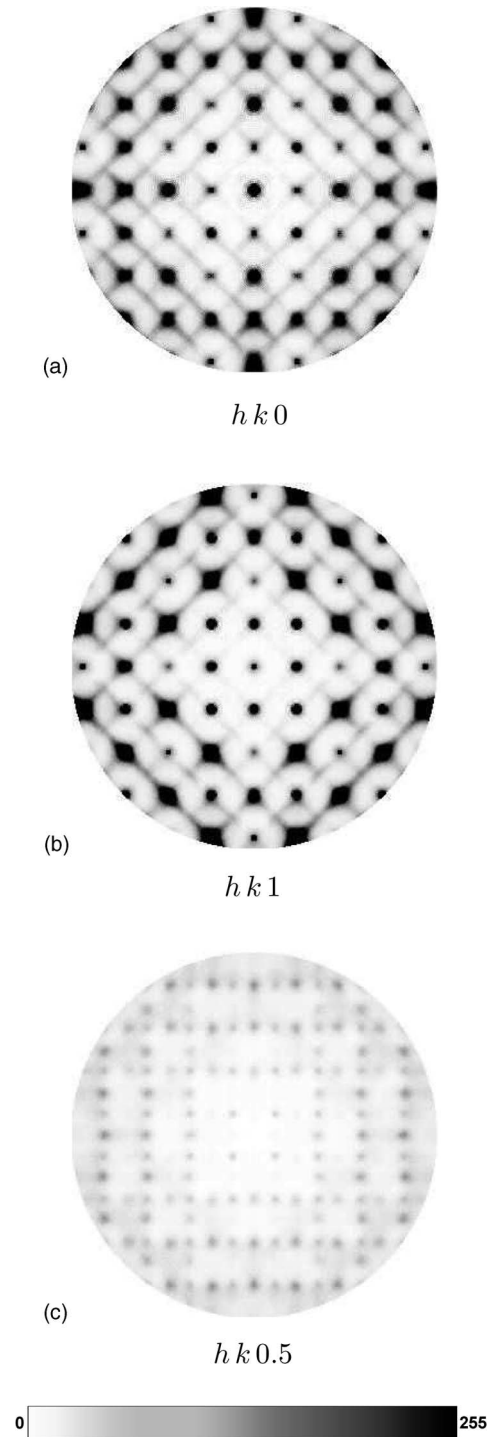$h\,k\,0$

(b)

$h\,k\,1$

(c)

$h\,k\,0.5$

0   255

FIG. 7. Calculated diffuse neutron scattering patterns for three sections of PZN obtained from the final Monte Carlo model.

sponding to zero electric field. First it should be noted that the domains of black (blue) arrows are larger at the expense of both the dark gray (pink) arrows and the out-of-plane vectors. It should also be noted that although the correlated domains of black (blue) or dark gray (pink) arrows do persist in successive layers rather more than in the corresponding simulation of Fig. 4, there is still only partial overlap, indicating that they are still essentially thin platelike nanoscale domains. While Figs. 8(a) and 8(b) are of sections nor-

TABLE III. Frequencies with which the different components of the 12-state vector quantity $\Psi_n(i,j,k)$ were present in the simulation corresponding to the system in an applied electric field.

$[uvw]$	$[011]$	$[101]$	$[110]$	$[01\bar{1}]$	$[0\bar{1}1]$	$[10\bar{1}]$
$[uvw]\times[111]$	2	2	2	0	0	0
Frequency	0.229	0.229	0.229	0.042	0.042	0.042

$[uvw]$	$[\bar{1}01]$	$[1\bar{1}0]$	$[\bar{1}10]$	$[0\bar{1}\bar{1}]$	$[\bar{1}0\bar{1}]$	$[\bar{1}\bar{1}0]$
$[uvw]\times[111]$	0	0	0	-2	-2	-2
Frequency	0.042	0.042	0.042	0.021	0.021	0.021

mal to $[1\bar{1}0]$ which contain large numbers of the field-enhanced $[110]$ vectors, Fig. 8(c) shows a section from the same distribution in a plane normal to $[110]$. This plane contains none of the vectors that have been enhanced by the applied field and so contains only very small domains of arrows directed along $\pm[1\bar{1}0]$.

Figure 8 shows the $hk0$ diffraction pattern for this polarized distribution. The intensity scale of this figure has been enhanced by a factor of about 2 compared to those in Fig. 7 in order to show the diffuse rods. The overall intensity in the rods has diminished compared to those in Fig. 7 but the reduction is only by a factor of about 2. In contrast the strong scattering around the Bragg positions has increased. These strong diffuse peaks around the Bragg positions now show an asymmetry (see peak labeled A), indicating that the $[110]$ direction is different from $[1\bar{1}0]$ direction. The figure also shows some evidence that the diffuse rods parallel to $[1\bar{1}0]$ (e.g., near label B) have a greater intensity than those parallel to $[110]$ (e.g., near label C), though the effect is not very marked. A further feature of the patterns is the splitting into two lobes of the diffuse peaks (see peak labeled D). The stronger peaks also show the same kind of splitting when viewed on a smaller scale. Such splitting, which is Huang-type scattering due to strain induced by the size-effect distortion, was noted by Xu et al.[14] in their x-ray experiment.

VI. SUMMARY AND CONCLUSION

In this paper we have described the development of an atom-based Monte Carlo simulation model which gives rise to a nanoscale polar domain structure envisaged to occur in PZN and similar relaxor ferroelectric materials. Calculated diffuse scattering patterns have been obtained from the simulations, and these are in good agreement with observed neutron diffuse scattering data. The model is based on important chemical considerations, most important of which is the fact the Pb ions must move away from their average site at the center of the 12-fold coordination polyhedron of O ions since at this position they cannot satisfy their valence requirements—i.e., the Pb atoms are grossly underbonded. A given Pb atom's correct apparent valence is most easily achieved by a shift in one of the 12 $\langle 110 \rangle$ directions towards one of its neighboring O ions. That the Pb atom shifts are directed along $\langle 110 \rangle$, and not $\langle 111 \rangle$ or $\langle 100 \rangle$, is clearly dem-
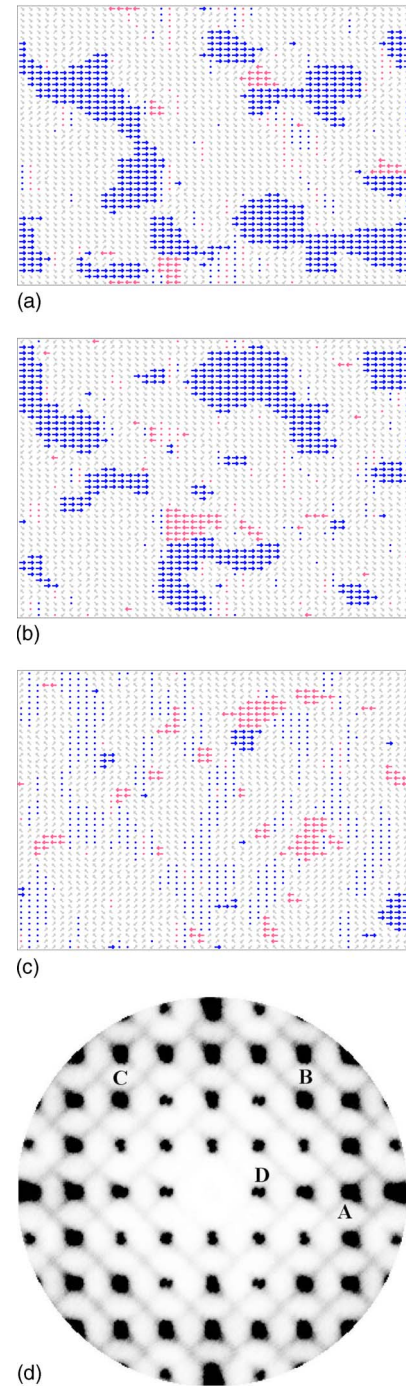

FIG. 8. (Color online) (a), (b) Distribution of Pb displacement vectors within two layers normal to $[1\bar{1}0]$ of the simulated structure in an electric field. The two layers are separated by $\sqrt{2}a_0$ along $[1\bar{1}0]$. $[001]$ is vertical and $[110]$ is horizontal. The black (blue) and dark gray (pink) arrows are in-plane vectors directed along $[110]$ and $[\bar{1}\bar{1}0]$, respectively. Light gray arrows are out-of-plane $\langle 110 \rangle$ vectors, while small circles are vectors normal to the plane. (c) A comparable layer normal to $[110]$ from the same distribution. In this layer $[001]$ is vertical and $[1\bar{1}0]$ is horizontal. Note the much smaller nanoscale domains. (d) The $hk0$ section of the diffraction pattern for this example. Features A, B, C, and D are described in the text.

onstrated by the systematic extinction of the intensity of the $h \pm k = 0$ diffuse rods in the observed diffraction patterns, Figs. 1(a) and 1(b).

These $\langle 110 \rangle$-type Pb shifts are found to be correlated to form nanoscale planar domains perpendicular to each of the six $\langle 110 \rangle$ directions. This is achieved in the model by a simple potential in which an energy E_2 is used to induce correlations in in-plane $\langle 110 \rangle$ directions and E_1 in in-plane $\langle 001 \rangle$ directions as given by Eqs. (3) and (4).

The distribution produced by this basic ordering scheme was then allowed to relax using size-effect distortions acting along $\langle 110 \rangle$ inter-Pb vectors. For this it was assumed that the distance between the centers was increased or decreased by an amount proportional to the scalar product of the two neighboring Pb shift vectors. This relaxation scheme was able to reproduce the asymmetric diffuse peak shapes evident in the observed data.

In all of the calculations the coordinates of the other (Nb/Zn and O) ions were included in a deterministic way based on the average of neighboring Pb positions. The inclusion of these other ions is crucial for the satisfactory reproduction of the diffraction patterns but they were not included directly in the ordering of the nanoscale polar domains.

There is a body of evidence obtained from consideration of which materials form relaxors and which do not that the chemical heterogeneity on the perovskite B sublattice plays an important role in the formation of the polar domains in relaxors. Burton *et al.*[19,20] describe how local B-site order can create over bonded and underbonded oxygens that then respectively repel or attract Pb ions. Alternatively it may be considered that the unlike charges on the B-site ions will create local electric fields that influence the Pb displacement direction. Such considerations would necessarily form the basis of any coupling between cation and polar ordering. Despite the fact that the FWHM of the two different kinds of diffuse peak in Fig. 1(c) indicate that the two types of order have a comparable range, no evidence that the two are directly linked has so far been revealed by the present diffuse scattering study. The present model used a short-range ordering scheme for the distribution of Nb and Zn that was quite independent of the polar domain ordering, and the level of agreement with observation is such that it must be concluded that any link between these distinct types of local order must result only in very subtle diffraction effects. Further development of the present model is in progress with a view to trying to establish whether the two may be directly linked, while making only subtle differences to the diffraction patterns.

The simulations reported here show clearly how it is possible to pack differently oriented planar $\langle 110 \rangle$ nanoscale domains into a three-dimensional structure and yet maintain average cubic symmetry. The nanoscale polar domains are found to be essentially one unit cell thick, and thicker domains would drastically affect the appearance of the diffuse scattering. Moreover, it is easy to see from the realizations how differently polarized domains can grow or dissolve simply by reorienting individual Pb shifts in cells on the periphery of the domain as a result of (for example) applying an external field. No diffusion is required. It is only necessary that a Pb atom relinquish its close chemical attachment to one of its coordinating oxygens and establish it with a different one. Such a mechanism gives insight into how the relaxor property of the material can remain even when the material passes through a phase transition or when there are different degrees of compositional segregation as discussed, for example, by Akbas and Davies.[16]

The example given in Sec. V in which the effect of an applied field was explored was also able to give insight into how the Pb atomic shifts which are directed along $\langle 110 \rangle$ directions could be reordered to give net polarization along [111] while maintaining many attributes of the nanoscale planar domain structure with local $\langle 110 \rangle$ polarization.

Despite the simplicity of the way that the non-Pb atoms have been treated in the study and the fact that the MC model itself has few adjustable parameters—the basic Pb shift parameter δ, the ordering energies E_1 and E_2, and the size-effect constant $k_{[110]}$—the calculated diffraction patterns show remarkably good agreement with the observed neutron data. There is little doubt that the model has captured the basic physics of the polar nanodomain formation. However, there are still aspects of the model that could be further improved, particularly with regard to applying detailed chemical constraints to all of the interionic vectors, and further work is planned in this direction.

ACKNOWLEDGMENTS

*Electronic address: welberry@rsc.anu.edu.au

[1] S.-E. Park and T. Shrout, J. Appl. Phys. **82**, 1804 (1997).

[2] Z.-G. Ye, M. Dong, and I. Zang, Ferroelectrics **229**, 223 (1999).

[3] Y.-H. Bing, A. Bokov, Z.-G. Ye, B. Noheda, and G. Shirane, J. Phys.: Condens. Matter **17**, 2493 (2005).

[4] R. Service, Science **275**, 1878 (1997).

[5] G. Burns and F.H. Dacol, Phys. Rev. B **28**, 2527 (1983).

[6] L. Cross, Ferroelectrics **76**, 241 (1987).

[7] P. Woodward and K. Baba-Kishi, J. Appl. Crystallogr. **35**, 233 (2002).

[8] W. Dmowski, M. Akbas, P. Davies, and T. Egami, J. Phys. Chem. Solids **61**, 229 (2000).

[9] T. R. Welberry, M. J. Gutmann, H. Woo, D. J. Goossens, G. Xu, C. Stock, W. Chen, and Z.-G. Ye, J. Appl. Crystallogr. **38**, 639 (2005).

[10] T. R. Welberry and B. D. Butler, J. Appl. Crystallogr. **27**, 205

(1994).

[11] T. R. Welberry, *Diffuse X-ray Scattering and Models of Disorder*, IUCr Monographs on Crystallography (Oxford University Press, Oxford, 2004).

[12] T. R. Welberry, Acta Crystallogr., Sect. A: Found. Crystallogr. **57**, 244 (2001).

[13] T. R. Welberry, D. J. Goossens, A. J. Edwards, and W. I. F. David, Acta Crystallogr., Sect. A: Found. Crystallogr. **57**, 101 (2001).

[14] G. Xu, Z. Zhong, Y. Bing, Z.-G. Ye, and G. Shirane, Nat. Mater. **5**, 134 (2006).

[15] N. E. Brese and M. O'Keeffe, Acta Crystallogr., Sect. B: Struct. Sci. **47**, 192 (1991).

[16] M. Akbas and P. Davies, J. Am. Ceram. Soc. **80**, 2933 (1997).

[17] B. D. Butler and T. R. Welberry, J. Appl. Crystallogr. **25**, 391 (1992).

[18] N. Metropolis, A. W. Rosenbluth, M. N. Rosenbluth, A. H. Teller, and E. Teller, J. Chem. Phys. **21**, 1087 (1953).

[19] B. P. Burton and E. Cockayne, Phys. Rev. B **60**, R12542 (1999).

[20] B. P. Burton, E. Cockayne, S. Tinte, and U. V. Waghmare, Phase Transitions **79**, 91 (2006).